FRONTIERS OF PHYSICS

RESEARCH ARTICLE
Volume 19 / Issue 3 / 33206 / 2024

Transmission-reflection decoupling of non-Hermitian photonic doping epsilon-near-zero media

Yongxing Wang (王勇幸)[1,2], Jizi Lin (林季资)[1,2], Ping Xu (须萍)[3,†]

1 Zhangjiagang Campus, Jiangsu University of Science and Technology, Zhangjiagang 215600, China
2 Department of physics, Jiangsu University of Science and Technology Suzhou Institute of Technology, Zhangjiagang 215600, China
3 School of Physical Science and Technology, Soochow University, Suzhou 215006, China
Corresponding author. E-mail: †pxu@suda.edu.cn
Received August 3, 2023; accepted October 30, 2023

ABSTRACT

We present a novel method to achieve the decoupling between the transmission and reflection waves of non-Hermitian doped epsilon-near-zero (ENZ) media by inserting a dielectric slit into the structure. Our method also allows for independent control over the amplitude and the phase of both the transmission and reflection waves through few dopants, enabling us to achieve various optical effects, such as perfect absorption, high-gain reflection without transmission, reflectionless high-gain transmission and reflectionless total transmission with different phases. By manipulating the permittivity of dopants with extremely low loss or gain, we can realize these effects in the same configuration. We also extend this principle to multi-port doped ENZ structures and design a highly reconfigurable and reflectionless signal distributor and generator that can split, amplify, decay and phase-shift the input signal in any desired way. Our method overcomes limitations of optical manipulation in doped ENZ caused by the interdependent nature of the transmission and reflection, and has potential applications in novel photonic devices.

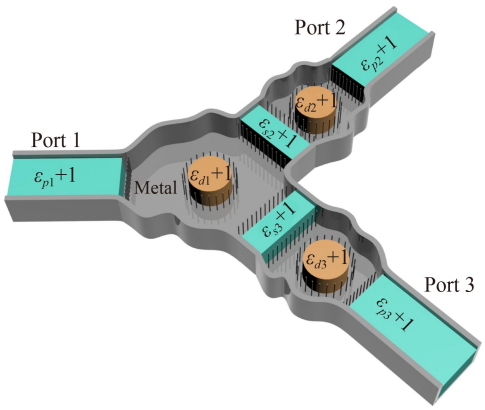

Keywords photonic doping, non-Hermitian, epsilon-near-zero media, transmission-reflection decoupling

1 Introduction

The ability to freely manipulate electromagnetic waves or light waves, an important carrier of energy and information, has always been a hot research topic. However, most optical media and systems exhibit coupled transmission and the reflection performances, and their amplitude and phase of transmission/reflection waves are also interdependent. Tuning one or more parameters of an optical medium or configuration usually leads to simultaneous changes in the power, amplitude and phase of the transmission and reflection waves, which limits the degree of freedom in optical manipulation and the information capacity of light. Recently, to overcome this bottleneck, some composite metasurfaces have been developed, which consist of arrays of artificial microstructures that can manipulate light in both transmission and reflection spaces [1–4], and even achieve simultaneous control of phase and amplitude [5, 6]. However, these metasurfaces are usually composed of large numbers of complex microstructures. To achieve specific functions, it is inevitable to adjust numerous unit cells. Moreover, the characteristics of most metasurfaces are geometrically dependent, which pose a challenge

Higher Education Press

https://doi.org/10.1007/s11467-023-1362-7

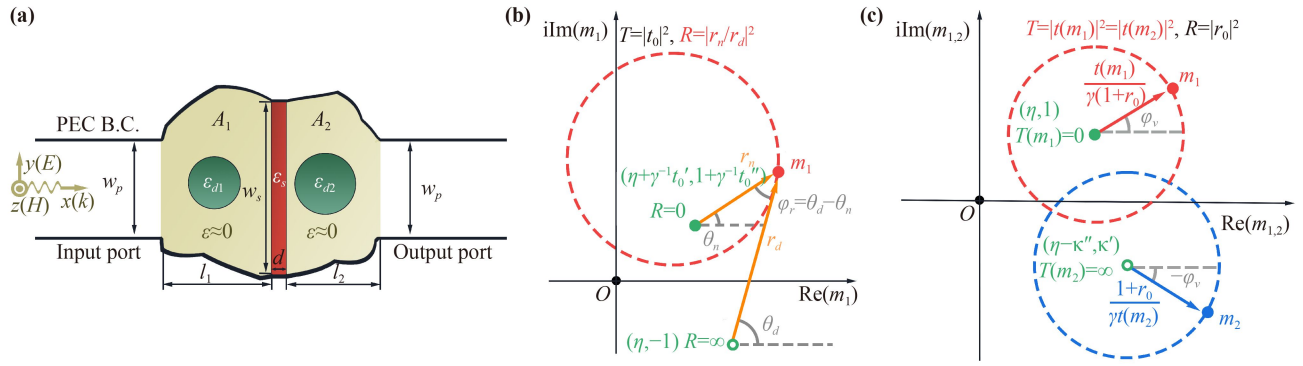

Fig. 1 **(a)** Diagrammatic sketch of the doped ENZ structure with two ports. **(b)** Diagram of the solutions of m_1 on the complex plane for a given reflectance R when the transmission coefficient is fixed as t_0. **(c)** Diagram of the solutions of m_1 and corresponding m_2 on the complex plane for a given transmittance T when the reflection coefficient is fixed as r_0.

for integration.

On the other hand, epsilon-near-zero media (ENZ) have attracted much interest due to their robust optical characteristics against geometric transformations [7–10]. In ENZ, the vanishing permittivity leads to a near-zero wavenumber, a wavelength much greater than its scale and the out-of-plane magnetic fields static in space. These features enable the control of the radiating direction [11, 12], phase distribution [13, 14], transmission performance [15, 16], and energy distribution [17] of light. More interestingly, ENZs exhibit extremely stable transmission performance irrespective of their geometric shape for TM polarized waves [15]. The spatially static magnetic fields also enable the photonic doping effect of ENZ such that the optical properties of the whole structure are tunable through one or few macroscopic dopants embedded in any position of the ENZ host [18–36]. These unconventional features make doped ENZs useful for engineering applications enabling the design of various doped-ENZ-based devices [37], such as power divider [38], antenna [12, 39], and filter [40]. Recently, increasing researchers are interested in non-Hermitian photonic doping ENZ with tailored loss and/or gain. With the introduction of optical non-Hermiticity in some components, the reconfigurability of doped ENZ is significantly improved [41], which brings more interesting effects, such as the enhancement of optical attenuation or amplification [42], coherent absorption [43, 44], and nonreciprocal transmission [42, 45]. Doping of ENZ provides a more convenient way for optical manipulation. Optical devices based on doped ENZ are convenient for integration and are expected to be applied in more fields, for their relatively simple structures and geometrically insensitive optical properties. However, out-of-plane fields with a constant amplitude in ENZ further intensify the correlation among the power, amplitude and phase of transmission and reflection waves.

Inspired by composite metasurfaces, we propose a novel method to break the correlation between the transmission and reflection waves of non-Hermitian doped ENZ by inserting a narrow dielectric slit. We demonstrate that both the amplitude and phase of both the reflection and transmission waves can be tuned independently through few dopants. Utilizing the amplification effect of loss or gain of dopants induced by resonance [42, 43], the adjustable range increases significantly. Moreover, we show that our method can be exploited to design a highly reconfigurable reflectionless signal distributor and generator based on a three-port doped ENZ waveguide structure.

2 Theories and analyses

We investigate the scattering properties of an arbitrarily shaped ENZ structure connecting two ports, as shown in Fig. 1(a). The structure consists of two ENZ regions (region 1 and region 2 with cross areas A_1 and A_2 respectively) separated by a dielectric slit with width w_s, thickness d and relative permittivity ε_s. The ENZ regions are connected to two ports with the same width w_p and relative permittivity ε_p. Each ENZ region contains a cylindrical dopant j $(j=1,2)$ with radius $\mathscr{R}_j$ and relative permittivity ε_j to control the reflection and transmission performance of the structure. The dopants are nonmagnetic and may exhibit dielectric loss or gain. The structure is bounded by perfect electric conductor (PEC) walls. We assume that a transverse magnetic polarized (TM) plane wave with angular frequency ω normally incident from the input port (the left port). If the time factor $\mathrm{e}^{-\mathrm{i}\omega\tau}$ is omitted, the magnetic field inside the input port, the slit and the output port (the right port) are expressed as

$$\boldsymbol{H}_i = H_0(\mathrm{e}^{\mathrm{i}k_p x} + r\mathrm{e}^{-\mathrm{i}k_p x})\boldsymbol{e}_z, \tag{1a}$$

$$\boldsymbol{H}_s = H_0[a\mathrm{e}^{\mathrm{i}k_s(x-l_1)} + b\mathrm{e}^{-\mathrm{i}k_s(x-l_1)}]\boldsymbol{e}_z, \tag{1b}$$

$$\boldsymbol{H}_o = H_0 t\mathrm{e}^{\mathrm{i}k_o(x-l_1-d-l_2)}\boldsymbol{e}_z, \tag{1c}$$

where $k_p = \sqrt{\varepsilon_p}k_0$ and $k_s = \sqrt{\varepsilon_s}k_0$ are wavenumbers in the two ports and the slit, respectively; $k_0 = \omega/c$ is the angular wavenumber in vacuum; and c is the velocity of light in vacuum; H_0 is the complex amplitude of the incident wave. t and r are the transmission coefficient and the reflection coefficient of the doped ENZ respectively. a and b are the complex amplitudes of the forward and backward waves in the slit normalized by H_0. Correspondingly, the electric fields in these regions are derived from $-\mathrm{i}\omega\varepsilon\boldsymbol{E} = \nabla \times \boldsymbol{H}$ as

$$\boldsymbol{E}_i = z_0 z_p H_0(\mathrm{e}^{\mathrm{i}k_p x} - r\mathrm{e}^{-\mathrm{i}k_p x})\boldsymbol{e}_y, \tag{2a}$$

$$\boldsymbol{E}_s = z_0 z_s H_0[a\mathrm{e}^{\mathrm{i}k_s(x-l_1)} - b\mathrm{e}^{-\mathrm{i}k_s(x-l_1)}]\boldsymbol{e}_y, \tag{2b}$$

$$\boldsymbol{E}_o = z_0 z_p H_0 t\mathrm{e}^{\mathrm{i}k_o(x-l_1-d-l_2)}\boldsymbol{e}_y. \tag{2c}$$

$z_p = 1/\sqrt{\varepsilon_p}$ and $z_s = 1/\sqrt{\varepsilon_s}$ are the relative impedances of the two ports and the slit, respectively, and z_0 is the impedance in vacuum. We can calculate r, a, b, t from continuous boundary condition and the integral form of Faraday's law of electromagnetic induction as $\boldsymbol{M}(r,a,b,t)^{\mathrm{T}} = (1,1,0,0)^{\mathrm{T}}$ where

$$\boldsymbol{M} = \begin{pmatrix} -1 & 1 & 1 & 0 \\ 1 & \alpha - \mathrm{i}m_1 & -\alpha - \mathrm{i}m_1 & 0 \\ 0 & D_+ & D_- & -1 \\ 0 & -\alpha D_+ & \alpha D_- & 1 - \mathrm{i}m_2 \end{pmatrix}; \tag{3}$$

$\alpha = z_s w_s / z_p w_p$, $D_\pm = \mathrm{e}^{\pm k_s d}$ and $m_j = k_0 \mu_{\mathrm{eff}j} A_j/(z_p w_p)$. Here the homogenized effective magnetic permeability $\mu_{\mathrm{eff}j}$ is calculated with $\mu_{\mathrm{eff}j} = 1 - \pi\mathscr{R}_j^2/A_j + 2\pi\mathscr{R}_j J_1(\sqrt{\varepsilon_{dj}}k_0\mathscr{R}_j)/[A_j\sqrt{\varepsilon_{dj}}k_0 J_0(\sqrt{\varepsilon_{dj}}k_0\mathscr{R}_j)]$ according to the theory of photonic doping [18], which is commonly used to describe the transmission and reflection properties of doped ENZs. However, $\mu_{\mathrm{eff}j}$ alone is not enough to capture the effects of other physical quantities that influence the transmission and reflection properties, such as A_j, w_p, z_p, and k_0. Therefore, we adopt the dimensionless parameter m_j that combines $\mu_{\mathrm{eff}j}$ and these quantities in a simple way. This parameter can characterize the ENZ region j more comprehensively and simplify our analysis. It is easy to see that m_j dominates both the transmission and reflection performance of the ENZ in region j. In this work, we name m_j as the transmission-reflection main control (TRMC) parameter of the ENZ in region j, and use m_j as the variable to describe the ENZ in region j. We can obtain expressions for the reflection coefficient r and the transmission coefficient t as a function of m_1 and m_2, by inverting matrix $\boldsymbol{M}$. The correlation between r and t depends on their Jacobian determinant calculated by

$$\det\left[\frac{\partial(r,t)}{\partial(m_1,m_2)}\right] = \frac{4\gamma^2(z_p w_p z_s w_s)^3[m_2 - (\eta - \mathrm{i})]}{\det^3(\boldsymbol{M})}, \tag{4}$$

where $\det(\boldsymbol{M}) = -2\mathrm{i}\alpha\gamma[\eta(m_1+m_2+2\mathrm{i}) - (m_1+\mathrm{i})(m_2+\mathrm{i}) + \alpha^2]$, $\gamma = -\sin(k_s d)/\alpha$ and $\eta = \alpha\cot(k_s d)$. When $k_s d \neq n\pi$ $(n = 0, \pm1, \pm2, \ldots)$, $m_2 \neq \eta - \mathrm{i}$ and $\det(\boldsymbol{M})$ is convergent or both $|\det(\boldsymbol{M})|^3$ and $|\gamma^2(m_2 - \eta - \mathrm{i})|$ are small quantities of the same order, the Jacobian determinant is nonzero, which means r and t are independent. When t is fixed as t_0, r can be expressed as a univalent complex function of m_1 or m_2

$$\begin{aligned} r &= -\frac{m_1 - (\eta + \gamma^{-1}t_0 + \mathrm{i})}{m_1 - (\eta - \mathrm{i})} \\ &= \gamma t_0[m_2 - (\eta - \mathrm{i})] - 1. \end{aligned} \tag{5}$$

On the complex plane of m_1, there are a zero point at $\eta - \gamma^{-1}t_0 + \mathrm{i}$ and a pole point at $\eta - \mathrm{i}$ of the reflection coefficient r. This means that the reflection wave disappears when $m_1 = \eta - \gamma^{-1}t_0 + \mathrm{i}$ and diverges when $m_1 = \eta - \mathrm{i}$. The transmission coefficient t_0 determines the location of the reflection zero point, but not the unique value of reflection coefficient r. Figure 1(b) shows the diagram of how r varies with m_1. We represent r as the negative ratio of the vector $\boldsymbol{r}_n$ and $\boldsymbol{r}_d$, where $\boldsymbol{r}_n$ is the vector from the zero point to m_1 and $\boldsymbol{r}_d$ is the vector from the pole point to m_1. Any reflectance $R = |r|^2$ from near zero to near infinity is achievable by tuning m_1. Accordingly, to ensure the permanent t_0, m_2 should also be tuned to meet Eq. (5). On the complex plane of m_2, the zero point maps to $\eta + 1/\gamma t_0 - \mathrm{i}$ which is also determined by t_0. The pole point maps to the point of infinity. Based on the resonance properties of dopants, a wide range of TRMC parameters m_1 and m_2, including near-infinite values, is available by doping the proper materials with low loss or gain. In this way, without affecting the transmission coefficient t_0, the reflectance is broadly tunable from near zero to near infinity by adjusting the parameters of the dopants embedded in both ENZ regions unless the zero point and the pole point coincide or both are at infinity. Both the transmission and reflection waves of the doped ENZ structure can be controlled independently. Fig. 1(b) also illustrates that the contour of the amplitude of any reflection coefficient $|r|$ $(\neq 0$ or $\infty)$ forms an Apollonius circle around the zero point or the pole point of r. The reflection phase $\varphi_r = \theta_n - \theta_d$ is represented as the angle between vectors $\boldsymbol{r}_n$ and $\boldsymbol{r}_d$. When m_1 moves along a contour of $|r|$, φ_r changes from $-\pi$ to π. We can achieve any reflection phase for any given $|r|$. The argument principle also supports this interpretation. Thus, the correlation between the amplitude and phase of the reflection wave is broken.

Similarly, for a determined reflection coefficient $r = r_0$, t is a univalent complex function of m_1 or m_2

$$t = \gamma(1 + r_0)[m_1 - (\eta + \kappa\mathrm{i})] = \frac{1 + r_0}{\gamma[m_2 - (\eta - \mathrm{i})]}, \tag{6}$$

where $\kappa = (1 - r_0)/(1 + r_0)$. On the complex plane of m_1, the transmission coefficient t vanishes at $\eta + \kappa\mathrm{i}$ and diverges at the point of infinity. While, if t is expressed

as a function of m_2, it vanishes at the point of infinity and diverges at $\eta - \mathrm{i}$. The reflection coefficient r_0 affect the location of the transmission zero point but it does not determine t uniquely. As illustrated in Fig. 1(c), on the plane of m_1, the contour of constant amplitude $|t|$ ($\neq 0$ or ∞) forms a circle with the zero point as the center and a radius proportional to $|t|$. On the plane of m_2, the corresponding contour mapped by Eq. (6) forms another circle with the pole point as the center and a radius inversely proportional to $|t|$. Based on the resonance effect, it is not difficult to obtain the TRMC parameter m_1 or m_2 with a value close to infinity by doping. Hence, when the reflection coefficient is fixed, the transmittance $T = |t|^2$ can also be tailored in a wide range from near zero to near infinity in theory. Meanwhile, the argument principle also enables the full angle tunability of the transmission phase φ_t for any given non-zero and non-divergent $|t|$. From the perspective of vector geometry in Fig. 1(c), φ_t is related to $\varphi_v(-\varphi_v)$, which is the angle of the vector from the zero (pole) point to the corresponding contour of $|t|$. They satisfy $\varphi_v = \pi + \varphi_t - \mathrm{Arg}(1 + r_0)$. When r_0 and $|t|$ are determined, φ_t can be tuned in any angle by changing φ_v. Therefore, the amplitude and the phase of transmission wave are no longer interrelated.

We further discuss the physical mechanism behind the decoupling of transmission and reflection. The incident and reflection waves superpose in ENZ region 1, which means the reflected waves depend on the magnetic field in ENZ region 1. Moreover, the transmitted wave is determined by the magnetic field in ENZ region 2. The magnetic fields in the two ENZ regions interact through the dielectric slit between them. The modes of magnetic fields in the dielectric slit paly a critical role in the correlation between the transmitted and reflected waves. If the single-pass phase shift in the slit satisfies $k_s d = n\pi$ ($n = 0, \pm 1, \pm 2, \ldots$), the magnetic fields in the slit and two ENZ regions are symmetric or antisymmetric with respect to the central axis of the slit, which cannot be changed by any photonic doping. Such symmetry of magnetic modes requires the transmission and reflection coefficients to be rigidly constrained by $1 + r = \pm t$. Of course, this covers the case of $n = 0$ in which no slits are introduced in the doped ENZ. Thus, the coupling of transmission and reflection waves of a doped ENZ mainly originates from the symmetry of magnetic fields between the input and output ports. Reasonably, introducing the dielectric slit whose parameters satisfy $k_s d \neq n\pi$ is an effective way to break this symmetry of magnetic fields. In addition, non-Hermitian dopants embedded in ENZ regions also play an important role in the decoupling of transmission and reflection, because they can overcome the other limitation for transmission and reflection waves brought by the law of energy conservation. Furthermore, these non-Hermitian dopants provide enough degrees of freedom to tune both the amplitude and phase of both transmission and reflection waves. Hence, we achieve the decoupling of transmission and reflection in the ENZ structure by introducing a proper dielectric slit and non-Hermitian dopants. The desired transmission and reflection waves can be obtained simultaneously through in proposed structure as demonstrated in Figs. 1(b) and (c).

Nevertheless, there are some noteworthy cases in which the decoupling of transmission and reflection is not valid, other than $k_s d = n\pi$. Firstly, when $m_2 = \eta - \mathrm{i}$, the zero point and the pole point of the reflection coefficient coincide. In this case, the transmission and reflection coefficients are fixed as $-2\mathrm{i}\gamma$ and -1 respectively regardless of m_1. This means that the magnetic field always vanishes in ENZ region 1 and the photonic doping effect in ENZ region 1 is completely invalid. This strange phenomenon is caused by the reflection features of gain-based ENZ in region 2. The reflection wave from ENZ region 2 is amplified to match the amplitude of the corresponding incident wave. Coincidentally, its reflection phase cancels out the round-trip phase shift in the slit and produces an extra phase shift of π. These lead to destructive interference of light in ENZ region 1, irrespective of the properties of ENZ region 1. Secondly, the transmission-reflection decoupling makes sense only when both r and t are convergent. From Eqs. (3), (5), and (6) we can easily prove that divergent r will result in the divergent t_0, and divergent t will lead to the divergent r_0. In fact, the divergence of r and t corresponds precisely to the laser mode induced by the constructive interference of multiple reflected and amplified waves in non-Hermitian optical media [46–50].

3 Results and discussion

3.1 Reconfigurability of reflection wave without transmission

We numerically analyze two specific cases in the section: near-zero transmission and near-zero reflection. First, we investigate how reflection wave of the structure can be reconfigured when the transmittance vanishes. According to Eq. (5), the reflection coefficient r depends on the divergence of TRMC parameters m_1 and m_2 when t_0 tends to zero. If m_2 is convergent, m_1 must be divergent and $r = -1$. ENZ region 1 acts as a perfect magnetic conductor. If m_2 diverges, the reflection zero point $\eta + \mathrm{i}$ and the pole point $\eta - \mathrm{i}$ are symmetrical with respect to the real axis. We assume the following parameters: $w_p = \lambda_0$, $w_s = 2\lambda_0$, $d = 0.1\lambda_0$, $A_1 = 2.5048\lambda_0^2$, $A_2 = 2.4411\lambda_0^2$, $\mathscr{R}_1 = \mathscr{R}_2 = 0.35\lambda_0$, and $\varepsilon_s = 1$. To block the transmission wave, the permittivity of dopant 2 is set to close to a state of resonance reflection. In our calculation, $\varepsilon_{d2} = 1.196$ gives a large $m_2 = -12122$. Figures 2(a) and (b) show the calculation results of the reflectance and the transmittance as a function of the real part ε'_{d1} and the imaginary part ε''_{d1} (the loss factor) of the relative

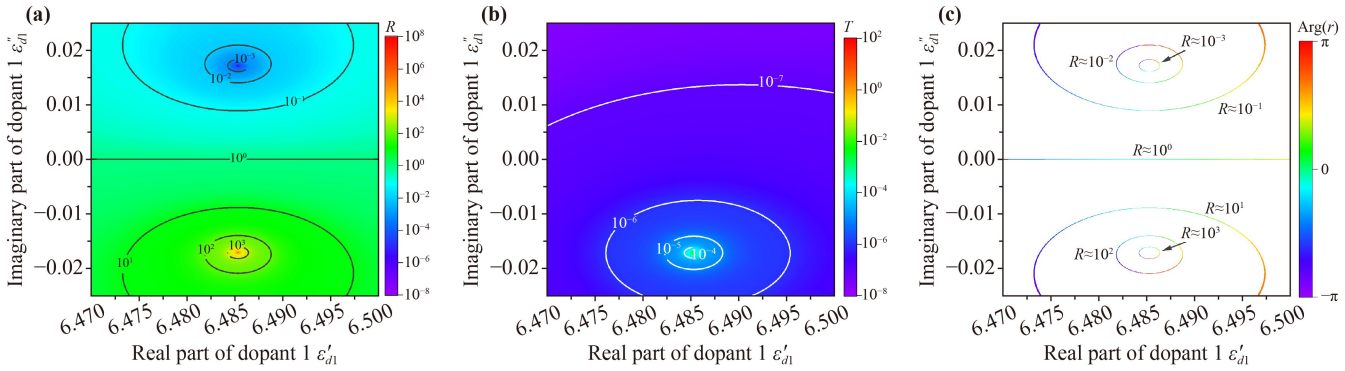

Fig. 2 Calculation results of **(a)** reflectance R and **(b)** transmittance T versus the real part of the relative permittivity of dopant 1 ε'_{d1} and the imaginary part of the relative permittivity of dopant 1 ε''_{d1} when $\varepsilon_{d2} = 1.196$. **(c)** Calculation results of the reflection phase for $R = 10^{-3} \pm 4 \times 10^{-5}$, $R = 10^{-2} \pm 2 \times 10^{-4}$, $R = 10^{-1} \pm 1 \times 10^{-3}$, $R = 1 \pm 1 \times 10^{-2}$, $R = 10^{1} \pm 1 \times 10^{-1}$, $R = 10^{2} \pm 2$ and $R = 10^{3} \pm 4 \times 10^{1}$.

permittivity of dopant 1. The reflectance varies continuously from 6.11×10^{-9} to 1.64×10^{8} with ε'_{d1} and ε''_{d1}. In our calculation domain, there is a reflection zero point and a reflection pole point symmetrically distributed on both sides of the real axis. In the most cases, waves are prevented from transmitting through the output port. When ε_{d1} approaches the reflection pole point, the transmittance increases to 12.89. As parameters get close to satisfying the laser mode condition, the resonant dopant 2 cannot block the transmission wave effectively, but the transmittance is still negligible compared with the reflectance. Hence, we obtain a wide range of reflectance from near-zero to near-infinity by adjusting dopant 2 with the near-zero transmittance. Moreover, Fig. 2(c) shows the distribution of the reflection phase near some specific reflectance values including $10^{-3}, 10^{-2}, 10^{-1}, 1, 10^{1}, 10^{2}$ and 10^{3}, which demonstrate the reconfigurability of the reflection phase. Any determined reflectance with any reflection phase is achievable by choosing the proper combination of ε'_{d1} and ε''_{d1}. We chose two values of the relative permittivity of dopant 1 close to the zero point $\varepsilon_{d1} = 6.485 + 0.017\mathrm{i}$ and the pole point $\varepsilon_{d1} = 6.485 - 0.017\mathrm{i}$ to conduct simulations using COMSOL Mutiphysics, as shown in Fig. 3. When the transmission wave is blocked, the zero reflection means that the energy of the incident wave is totally absorbed, as shown by the magnetic field distribution illustrated in Fig. 3(a). Figure 3(b) plots the amplitude of the magnetic fields distributed along the gray dashed line in (a). Clearly, in the input port, the incident wave with amplitude H_0 is almost unaffected, which means that there are almost no reflection waves in the doped ENZ structure. Meanwhile, in the other port, the amplitude of the transmission wave is less than $0.001H_0$. When $\varepsilon_{d1} = 6.485 - 0.017\mathrm{i}$, the reflection wave is amplified to about $101H_0$, which interferes with the incident wave. Because the amplitude of the reflection wave is much greater than that of the incident wave, the interference effect is not significant [Figs. 3(c) and (d)].

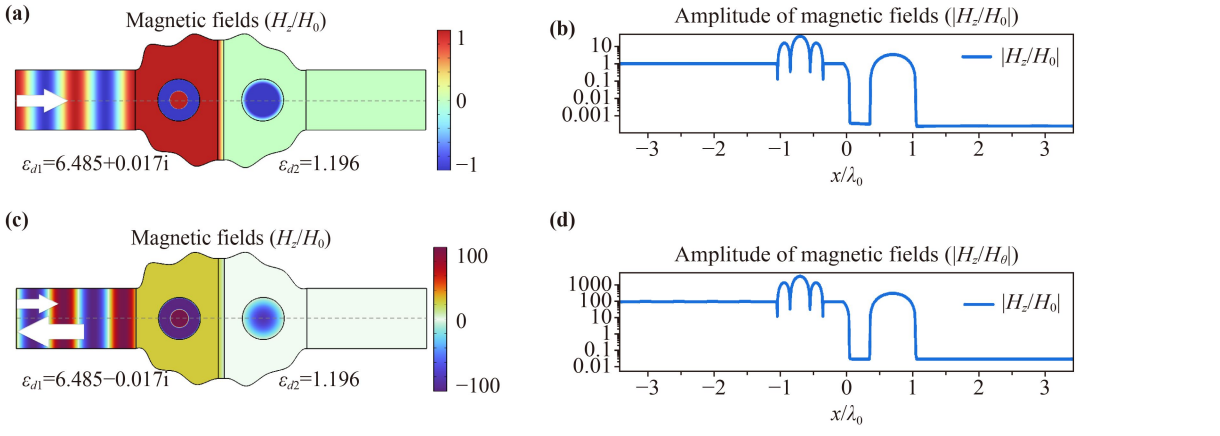

Fig. 3 **(a)** Simulation results of the distribution of magnetic fields in the ENZ structure for perfect absorption. **(b)** The corresponding distribution of the amplitude of magnetic fields along the gray dashed line in (a). **(c)** Simulation results of the distribution of magnetic fields in the ENZ structure for amplified reflection with extremely low transmission. **(d)** The corresponding distribution of the amplitude of magnetic fields along the gray dashed line in (c).

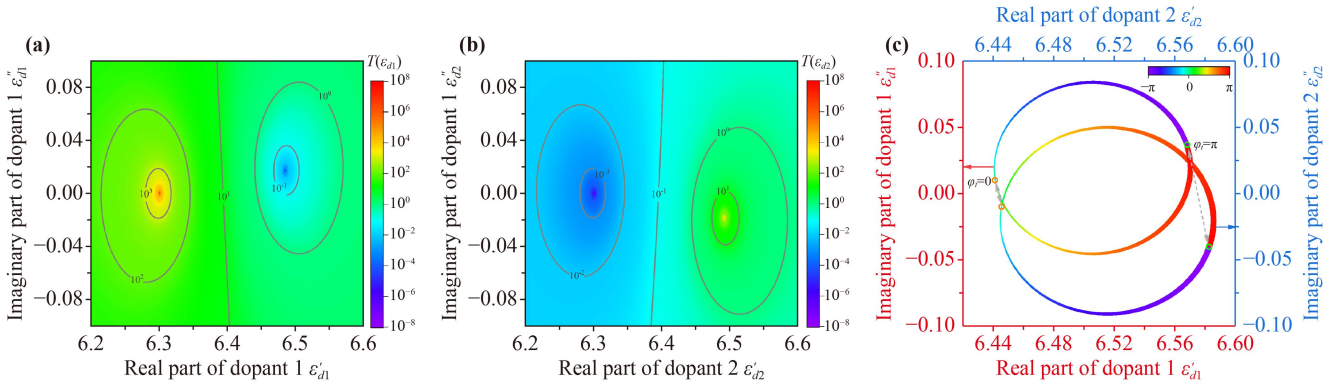

Fig. 4 Calculation results of the transmittance T versus **(a)** the real part and imaginary part of the relative permittivity of dopant 1 and **(b)** that of dopant 2 for reflectance $R = 0$. **(c)** Distributions of phase as a function of the real part and imaginary part of the relative permittivity of dopant 1 depicted by the red coordinate system and that of dopant 2 depicted by the blue coordinate system when the transmittance $T = 1 \pm 0.01$.

Although the amplitude of the transmission wave is enhanced to $0.028H_0$, the impact is still trivial. By changing the permittivity of dopant 1, we achieved perfect absorption and amplified reflection waves with near-zero transmission.

3.2 Reconfigurability of transmission wave without reflection

Next, we numerically analyze how the transmission wave can be reconfigured without reflection. To obtain the near-zero reflectance, dopants in both regions should be tuned to satisfy $[m_1 - (\eta + \mathrm{i})][m_2 - (\eta - \mathrm{i})] = \gamma^{-2}$, which is different from the case of near-zero transmission. In Fig. 4(a), we calculated the transmittance of the doped ENZ structure as a function of ε_{d1}, $T(\varepsilon_{d1})$, when the reflectance is close to zero. We use the same parameters as in Figs. 2 and 3 except for the permittivity of dopants. In the calculation domain, $T(\varepsilon_{d1})$ is tunable in a wide range. The transmission zero point is near $\varepsilon_{d1} = 6.485 + 0.017\mathrm{i}$, which agrees with the above calculation for the case of $\varepsilon_{d2} = 1.196$. Due to the resonance effect of dopant 1, the transmission pole point is mapped from the infinity point of m_1 to a point on the real axis of ε_{d1} near 6.301. Correspondingly, if we express the reflectionless transmittance as a function of ε_{d2}, the transmission zero point is mapped to near $\varepsilon_{d2} = 6.301$ and the pole point is mapped to near $\varepsilon_{d1} = 6.492 - 0.019\mathrm{i}$, as shown in Fig. 4(b). Near the transmission pole point, $T(\varepsilon_{d2})$ varies more sharply than $T(\varepsilon_{d1})$, which requires a higher accuracy for ε_{d2}. In contrast, near the transmission zero point, $T(\varepsilon_{d2})$ varies more gently than $T(\varepsilon_{d1})$, which means that ε_{d1} must be more accurate. Figures 5(a) and (b) show the simulation results of the amplification of the transmission wave with extremely low reflection. We choose $\varepsilon_{d1} = 6.202 - 0.046\mathrm{i}$ to obtain $T(\varepsilon_{d1}) = 71.24$. Based on $T(\varepsilon_{d1}) = T(\varepsilon_{d2})$ and $\varphi_t(\varepsilon_{d1}) = \varphi_t(\varepsilon_{d2})$, we find the corresponding dopant 2 with $\varepsilon_{d2} = 6.500 - 0.0175\mathrm{i}$ from the

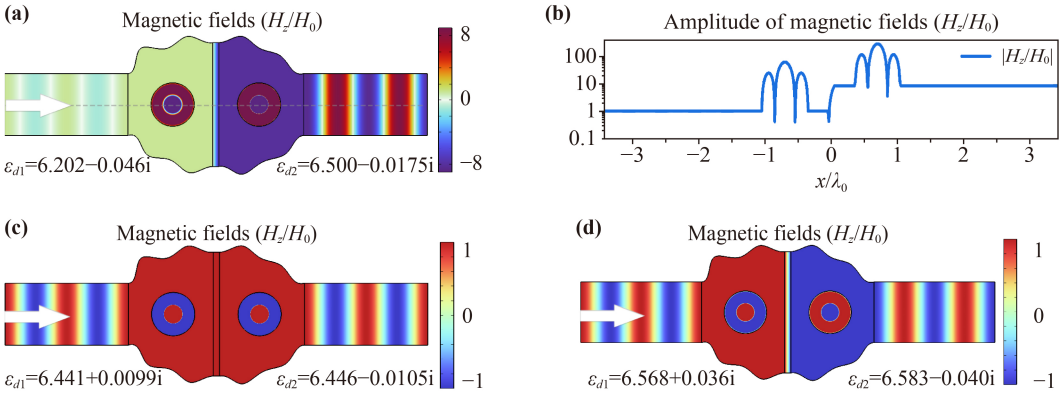

Fig. 5 **(a)** Simulation results of the distribution of magnetic fields in the ENZ structure for the amplified transmission with extremely low reflection. **(b)** The corresponding distribution of the amplitude of magnetic fields along the gray dashed line in (a). Simulation results of the distribution of magnetic fields in the ENZ structure for the reflectionless total transmission with **(c)** near-zero phase advance and **(d)** a π-phase advance.

calculation results. The simulated amplitude of the transmission wave is approximately $8.45H_0$, which matches the calculation results. The reflection wave is effectively suppressed. We implement a cascadable signal amplifier that can be useful for signal processing using the doped ENZ structure. As a result, the transmittance and reflectance are decoupled, which allows the transmittance to be tuned in a very broad range by adjusting two dopants while maintaining a negligible reflectance.

In addition, for any given transmittance other than the zero point and the pole point in the calculation domain, all the conforming ε_{d1} and corresponding ε_{d2} are respectively on a curve enclosing the zero or the pole point. On any curve with a constant T, different values of ε_{d1} or ε_{d2} indicate different transmission phases. In Fig. 4(c), we show the calculation results of the transmission phase as a function of ε_{d1}, $\varphi_t(\varepsilon_{d1})$, and that of ε_{d2}, $\varphi_t(\varepsilon_{d2})$, when $T \approx 1$ with $R \approx 0$. One can obtain any transmission phase ranging from $-\pi$ to π by simultaneously tuning ε_{d1} and ε_{d2}. For example, when we want the transmission wave to be in phase with the incident wave, we find from the calculation results that we need $\varepsilon_{d1} = 6.441 + 0.0099\mathrm{i}$ and $\varepsilon_{d2} = 6.446 - 0.0105\mathrm{i}$. Conversely, if we want the transmission wave to be out of phase with the incident wave, we need $\varepsilon_{d1} = 6.568 + 0.036\mathrm{i}$ and $\varepsilon_{d2} = 6.583 - 0.040\mathrm{i}$. Figures 5(c) and (d) demonstrate the simulation results of magnetic field of the ENZ structure when the transmission wave is in and out of phase with the incident wave respectively. By proper doping, reflectionless total transmission with the expected phase is obtained. These results show that the amplitude and the phase of the transmission wave are also decoupled.

Specifically, in our calculation domain, we notice that there are two time-reversal symmetric reflectionless total transmission modes where both dopants are pure dielectric with $\varepsilon_{d1} = 6.444$, $\varepsilon_{d2} = 6.448$ $(m_1 = m_2 = -0.47)$ or $\varepsilon_{d1} = 6.567$, $\varepsilon_{d2} = 6.582$ $(m_1 = m_2 = -5.99)$. They are two discrete resonance total transmission modes formed by destructive interference of multiple reflection waves [35]. Other reflectionless total transmission modes without time-reversal symmetry, in addition to the interference effect, involves energy exchanges due to the balanced loss and gain of dopants, which requires m_1 and m_2 to be PT symmetrical [42, 45, 46]. In our calculations, the difference between ε_{d1} and $\varepsilon_{d2}^{\star}$ is compensated by the geometric asymmetry. The total transmission modes induced by resonance can be regarded as some special cases of the PT symmetrical total transmission. In the non-Hermitian system, reflectionless total transmission modes degenerated by their transmission phases are continuous, which can be extended to other reflectionless modes with any fixed transmittance. Due to the periodicity of the resonance states of electromagnetic fields in dopants, these continuous modes will recur outside our calculation domains.

4 Applications in reflectionless signal distributor and generator

One can generalize the principle of transmission-reflection decoupling and the reconfigurability of amplitudes and phases to structures of doped ENZ with multiple ports. Since the number of ports does not affect its physical essence, we expect that the S-parameters of non-Hermitian doped ENZ with multiple ports will be uncorrelated and reconfigurable in their amplitude and phase when several slits are introduced. To demonstrate this, we propose a scheme to realize a highly reconfigurable signal distributor and generator using a structure of non-Hermitian doped ENZ with slits as illustrated in Fig. 6(a). The structure is composed of three ENZ regions labeled by $j = 1, 2, 3$. They are separated by two slits. Each ENZ region contains a dopant and connects to a port. Port 1 connecting to region 1 is the input port. Ports 2 and 3 connecting to regions 2 and 3 are two output ports. S_{11} denotes the reflection coefficient. S_{21} and S_{31} are the transmission coefficients of ports 2 and 3 respectively. According to the universal expression of S-parameters of doped ENZ with multiple ports and slits [36]. We find that when the reflection coefficient $S_{11} = 0$, the two transmission coefficients can be simplified into a very concise form similar to Eq. (6):

$$S_{j1} = \frac{1}{\gamma_j[m_j - (\eta_j - \mathrm{i})]}, \quad j = 2, 3, \tag{7a}$$

with

$$m_1 = \mathrm{i} - \sum\nolimits_{j=2}^{3}[(m_j + \mathrm{i})\cos(k_{sj}d_j)] + \frac{z_{sj}w_{sj}}{z_{p1}w_{p1}}\sin(k_{sj}d_j), \tag{7b}$$

where $m_j = k_0\mu_{\mathrm{eff}j}A_j/(z_{pj}w_{pj})$; $\mu_{\mathrm{eff}j}$ and A_j are the effective permeability and the cross-sectional area of ENZ region j, respectively; z_{pj} and w_{pj} are the relative impedance and the width of port j, respectively; z_{sj}, k_{sj}, w_{sj} and d_j are the relative impedance, wavenumber, width and thickness of the slit between regions 1 and j, respectively; $\gamma_j = -z_{pj}w_{pj}\sin(k_{sj}d_j)/(z_{sj}w_{sj})$; $\eta = z_{sj}w_{sj}\cot(k_{sj}d_j)/(z_{pj}w_{pj})$. Since these ports and slits are nonmagnetic, their relative permittivites are $\varepsilon_{pj} = z_{pj}^{-2}$ and $\varepsilon_{sj} = z_{sj}^{-2}$, respectively. The dopant in region j, dopant j with relative permittivity ε_{dj}, exhibits a circular cross section with the radius $\mathscr{R}_j$. As shown in Eq. (7a), the transmission coefficient S_{j1} is expressed as a univalent function of m_j. One can obtain any designed transmission coefficients S_{21} and S_{31} by choosing suitable dopants 2 and 3 respectively, and then find a matched dopant 1 to eliminate the reflection wave according to Eq. (7b). The incident wave can be split, amplified, decayed and phase shifted by any means with near-zero reflection through the signal distributor and generator.

Further, we construct this ENZ-based signal distributor

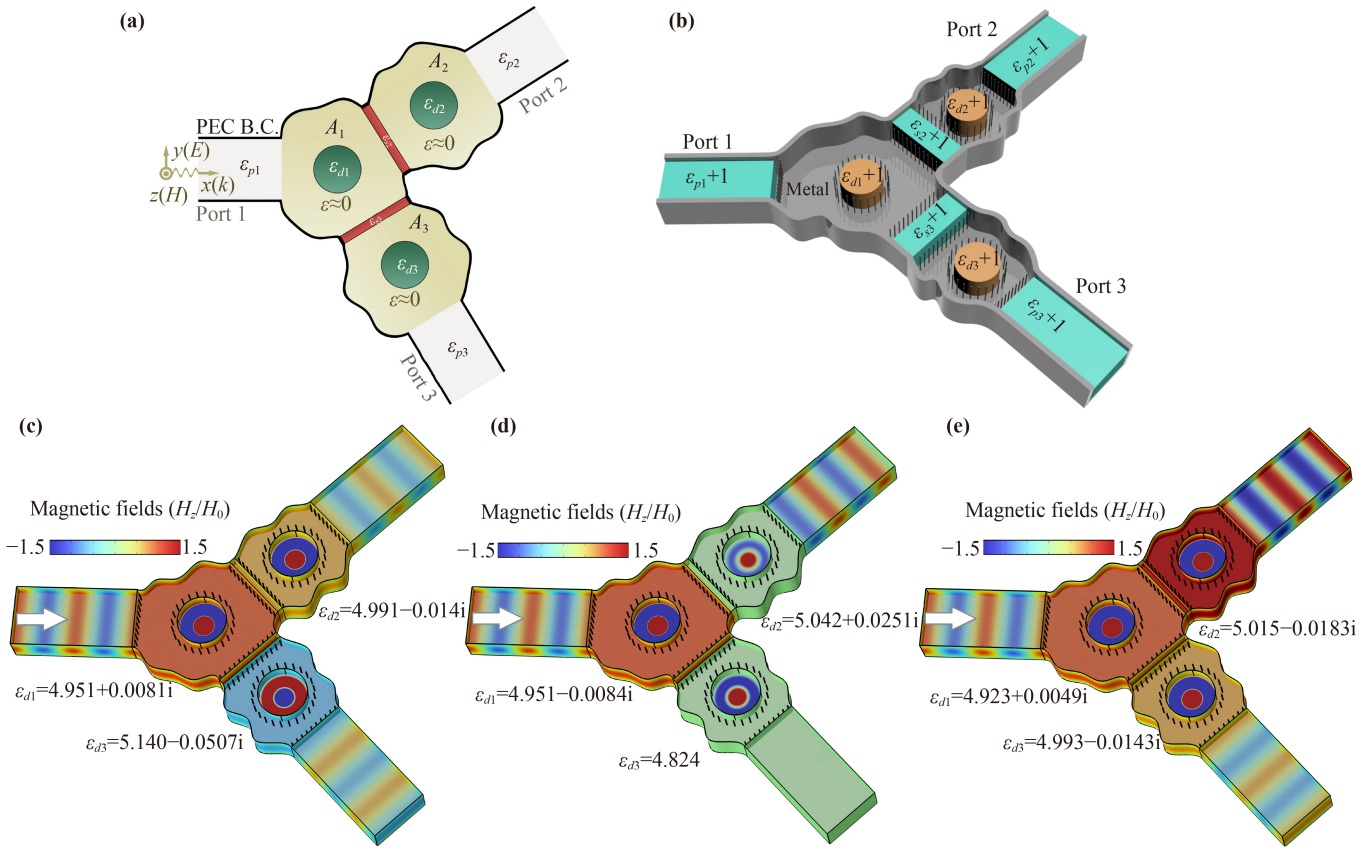

Fig. 6 Plane **(a)** and three-dimensional **(b)** diagrammatic sketch of the highly reconfigurable reflectionless signal distributor and generator. Simulation results of the magnetic field distribution in the signal distributor and generator when **(c)** the power of the incident wave is equally distributed into two output ports with opposite transmission phases, **(d)** when the incident wave is totally distributed into one output port with $\varphi_{21} = \pi/2$ and **(e)** when the incident wave is amplified in one output port and decayed in another output port with the same phase.

and generator through several interconnected three-dimensional metal waveguides that work at TE_{10} mode [18, 32–34], as shown in Fig. 6(b). The top metal wall of the waveguide structure is removed. The effective relative permittivity for TE_{10} mode is $\varepsilon_{\mathrm{eff}} = \varepsilon_f - (c\pi/\omega h)^2$, where ε_f is the relative permittivity of the filler and h is the height of the waveguide. We fill the three irregular-shaped regions with air ($\varepsilon_f = 1$) and set the height and frequency to satisfy $c\pi/(\omega h) = 1$, creating lossless ENZ host media at the cutoff frequency of TE_{10} mode. We also fill media with relative permittivities $\varepsilon_{pj} + 1$, $\varepsilon_{sj} + 1$ and $\varepsilon_{dj} + 1$ in corresponding regions of ports, slits and dopants, respectively, to achieve the desired effective relative permittivities ε_{pj}, ε_{sj} and ε_{dj} for TE_{10} mode. To prevent higher order modes from interfering, some thin metal rods are inserted near interfaces between different media.

We numerically simulate three cases with different transmission requirements of the signal distributor and generator constructed by the TE_{10} waveguide structure using the following parameters: $w_{p1} = w_{p2} = w_{p3} = \lambda_0$, where λ_0 is the working wavelength in vacuum; $w_{s2} = w_{s3} = 1.2\lambda_0$; $d_1 = d_2 = 0.1\lambda_0$; $h = c\pi/\omega = 0.5\lambda_0$; $\mathscr{R}_1 = \mathscr{R}_2 = \mathscr{R}_3 = 0.4\lambda_0$; $A_1 = 2.986\lambda_0^2$; $A_2 = A_3 = 1.667\lambda_0^2$; $z_{p1} = z_{p2} = z_{p3} = z_{s2} = z_{s3} = 1$; $k_{s2} = k_{s3} = k_0$. We use PECs to simulate metal sidewalls of the waveguide structure and introduce a total of 104 thin PEC rods with cross section area $7.854\times10^{-5}\lambda_0^2$ near interfaces between different media. In the first case, we split the incident wave into two output ports with equal power and opposite phases. We achieve this by using $\varepsilon_{d2} = 4.991 - 0.014\mathrm{i}$ and $\varepsilon_{d3} = 5.140 - 0.0507\mathrm{i}$ for dopants 2 and 3, and $\varepsilon_{d1} = 4.951 + 0.0081\mathrm{i}$ for dopant 1 to eliminate reflection. Figure 6(c) shows the simulated magnetic field distribution for this case. The transmission waves in ports 2 and 3 have the same amplitude $\sqrt{2}H_0$ where H_0 is the incident wave amplitude. The phase difference between port 1 and port 2 is zero, while the phase difference between port 1 and port 3 is π. Meanwhile, there almost no reflection from port 1. In the second case, we want total transmission through port 2 with a phase shift $\varphi_{21} = \pi/2$, no transmission through port 3 and no reflection through port 1. We achieve this by using $\varepsilon_{d1} = 4.951 - 0.0084\mathrm{i}$, $\varepsilon_{d2} = 5.042 + 0.0251\mathrm{i}$ and $\varepsilon_{d3} = 4.824$ for dopants 1, 2 and 3. Such function is demonstrated by the simulated magnetic field distribution in Fig. 6(d).

Interestingly, by choosing proper dopants, the structure can even generate an amplified and a decayed reflectionless transmission signal simultaneously. In the third case, we amplify the incident wave in port 2 and decay it in port 3. By using dopants 1, 2 and 3 with $\varepsilon_{d1} = 4.923 - 0.0049\mathrm{i}$, $\varepsilon_{d2} = 5.015 - 0.0183\mathrm{i}$ and $\varepsilon_{d3} = 4.993 - 0.0143\mathrm{i}$, the amplitude of the transmission wave in port 2 is amplified to $1.5H_0$ and that in port 3 decays to $0.75H_0$ [Fig. 6(e)]. In port 1, the reflection wave is also blocked effectively. The designed signal distributor and generator exhibits ultrahigh reconfigurability and potential applications in transmission and processing of optical signals.

5 Conclusion

We have demonstrated a novel way of manipulating optical waves by exploiting the properties of non-Hermitian doped ENZ structures with slits. We have shown that a dielectric slit in the ENZ structure can break the correlation between the transmission and reflection waves and allows us to control their amplitude and phase independently by adjusting the permittivity of few dopants. We have achieved various optical effects such as perfect absorption, high-gain reflection without transmission, reflectionless high-gain transmission and total transmission with phase modulation, by choosing appropriate values of permittivity with tailored low loss or gain for dopants. We have also extended our approach to doped ENZ structures with multiple slits and ports, and designed a highly reconfigurable and reflectionless signal distributor and generator based on a three-port ENZ waveguide structure. This device can distribute, amplify and phase-shift the incident wave in any desired way, which is useful for various applications such as optical communication and signal processing. Our work overcomes the restrictions of doped ENZ imposed by the correlation between the transmission and reflection waves as well as that between amplitudes and phases for freer optical manipulation, opening up a new avenue for designing novel optical devices based on non-Hermitian doped ENZ structures.

Declarations The authors declare that they have no competing interests and there are no conflicts.

Acknowledgements This work was supported by the National Natural Science Foundation of China (Nos. 12104191 and 11204195), the Natural Science Research of Jiangsu Higher Education Institutions of China (No. 21KJB140006), and the Priority Academic Program Development of Jiangsu Higher Education Institutions.

References

1. L. Bao, X. Fu, R. Y. Wu, A. Ma, and T. J. Cui, Full-space manipulations of electromagnetic wavefronts at two frequencies by encoding both amplitude and phase of metasurface, *Adv. Mater. Technol.* 6(4), 2001032 (2021)
2. Z. Li, J. Zhang, J. Liu, L. Liu, X. Wang, M. Premaratne, J. Yao, and W. Zhu, Independent manipulation of aperture and radiation fields in a transmission-reflection integrated complex-amplitude metasurface, *Adv. Mater. Technol.* 8(6), 2201192 (2023)
3. L. Deng, Z. Li, Z. Zhou, Z. He, Y. Zeng, G. Zheng, and S. Yu, Bilayer-metasurface design, fabrication, and functionalization for full-space light manipulation, *Adv. Opt. Mater.* 10(7), 2102179 (2022)
4. T. Cai, G. M. Wang, S. W. Tang, H. X. Xu, J. W. Duan, H. J. Guo, F. X. Guan, S. L. Sun, Q. He, and L. Zhou, High-efficiency and full-space manipulation of electromagnetic wave fronts with metasurfaces, *Phys. Rev. Appl.* 8(3), 034033 (2017)
5. C. Zheng, H. Li, J. Li, J. Li, Z. Yue, F. Yang, Y. Zhang, and J. Yao, All-dielectric metasurface for polarization selective full-space complex amplitude modulations, *Opt. Lett.* 47(17), 4291 (2022)
6. G. Li, H. Shi, J. Yi, B. Li, A. Zhang, and Z. Xu, Transmission–reflection-integrated metasurfaces design for simultaneous manipulation of phase and amplitude, *IEEE Trans. Antenn. Propag.* 70(7), 6072 (2022)
7. I. Liberal and N. Engheta, Near-zero refractive index photonics, *Nat. Photonics* 11(3), 149 (2017)
8. N. Kinsey, C. DeVault, A. Boltasseva, and V. M. Shalaev, Near zero-index materials for photonics, *Nat. Rev. Mater.* 4(12), 742 (2019)
9. X. Niu, X. Hu, S. Chu, and Q. Gong, Epsilon-near-zero photonics: A new platform for integrated devices, *Adv. Opt. Mater.* 6(10), 1701292 (2018)
10. J. Y. Wu, Z. T. Xie, Y. H. Sha, H. Y. Fu, and Q. Li, Epsilon near-zero photonics: Infinite potentials, *Photon. Res.* 9(8), 1616 (2021)
11. S. Enoch, G. Tayeb, P. Sabouroux, N. Guerin, and P. Vincent, A metamaterial for directive emission, *Phys. Rev. Lett.* 89(21), 213902 (2002)
12. J. J. Yang, Y. Francescato, S. A. Maier, F. Mao, and M. Huang, Mu and epsilon near zero metamaterials for perfect coherence and new antenna designs, *Opt. Express* 22(8), 9107 (2014)
13. A. Alù, M. G. Silveirinha, A. Salandrino, and N. Engheta, Epsilon-near-zero metamaterials and electromagnetic sources: Tailoring the radiation phase pattern, *Phys. Rev. B* 75(15), 155410 (2007)
14. G. Briere, B. Cluzel, and O. Demichel, Improving the transmittance of an epsilon-near-zero-based wavefront shaper, *Opt. Lett.* 41(19), 4542 (2016)
15. M. Silveirinha and N. Engheta, Tunneling of electromagnetic energy through subwavelength channels and bends using epsilon-near-zero materials, *Phys. Rev. Lett.* 97(15), 157403 (2006)
16. J. Luo and Y. Lai, Anisotropic zero-index waveguide with arbitrary shapes, *Sci. Rep.* 4(1), 5875 (2014)
17. M. M. Sadeghi, H. Nadgaran, and H. Y. Chen, Perfect field concentrator using zero index metamaterials and perfect electric conductors, *Front. Phys.* 9(1), 90 (2014)
18. I. Liberal, A. M. Mahmoud, Y. Li, B. Edwards, and N. Engheta, Photonic doping of epsilon-near-zero media,

Science 355(6329), 1058 (2017)
19. M. Silveirinha and N. Engheta, Design of matched zero index metamaterials using nonmagnetic inclusions in epsilon-near-zero media, *Phys. Rev. B* 75(7), 075119 (2007)
20. V. C. Nguyen, L. Chen, and K. Halterman, Total transmission and total reflection by zero index metamaterials with defects, *Phys. Rev. Lett.* 105(23), 233908 (2010)
21. Y. Xu and H. Chen, Total reflection and transmission by epsilon-near-zero metamaterials with defects, *Appl. Phys. Lett.* 98(11), 113501 (2011)
22. K. Zhang, J. Fu, L. Y. Xiao, Q. Wu, and L. W. Li, Total transmission and total reflection of electromagnetic waves by anisotropic epsilon-near-zero metamaterials embedded with dielectric defects, *J. Appl. Phys.* 113(8), 084908 (2013)
23. Y. Wu and J. Li, Total reflection and cloaking by zero index metamaterials loaded with rectangular dielectric defects, *Appl. Phys. Lett.* 102(18), 183105 (2013)
24. Y. Huang and J. Li, Total reflection and cloaking by triangular defects embedded in zero index metamaterials, *Adv. Appl. Math. Mech.* 7(2), 135 (2015)
25. J. Hao, W. Yan, and M. Qiu, Super-reflection and cloaking based on zero index metamaterial, *Appl. Phys. Lett.* 96(10), 101109 (2010)
26. J. Luo, P. Xu, L. Gao, Y. Lai, and H. Chen, Manipulate the transmissions using index-near-zero or epsilon-near-zero metamaterials with coated defects, *Plasmonics* 7(2), 353 (2012)
27. T. Wang, J. Luo, L. Gao, P. Xu, and Y. Lai, Hiding objects and obtaining Fano resonances in index-near-zero and epsilon-near-zero metamaterials with Bragg-fiber-like defects, *J. Opt. Soc. Am. B* 30(7), 1878 (2013)
28. A. M. Mahmoud and N. Engheta, Wave–matter interactions in epsilon-and-mu-near-zero structures, *Nat. Commun.* 5(1), 5638 (2014)
29. I. Liberal, Y. Li, and N. Engheta, Reconfigurable epsilon near-zero metasurfaces via photonic doping, *Nanophotonics* 7(6), 1117 (2018)
30. L. Zhao, Y. Feng, B. Zhu, and J. Zhao, Electromagnetic properties of magnetic epsilon-near-zero medium with dielectric dopants, *Opt. Express* 27(14), 20073 (2019)
31. I. Liberal, M. Lobet, Y. Li, and N. Engheta, Near-zero index media as electromagnetic ideal fluids, *Proc. Natl. Acad. Sci. USA* 117(39), 24050 (2020)
32. Z. Zhou, Y. Li, E. Nahvi, H. Li, Y. He, I. Liberal, and N. Engheta, General impedance matching via doped epsilon-near-zero media, *Phys. Rev. Appl.* 13(3), 034005 (2020)
33. Z. Zhou, Y. Li, H. Li, W. Sun, I. Liberal, and N. Engheta, Substrate-integrated photonic doping for near-zero-index devices, *Nat. Commun.* 10(1), 4132 (2019)
34. Z. H. Zhou, H. Li, W. Y. Sun, Y. J. He, I. Liberal, N. Engheta, Z. H. Feng, and Y. Li, Dispersion coding of ENZ media via multiple photonic dopants, *Light Sci. Appl.* 11(1), 207 (2022)
35. E. Nahvi, M. J. Mencagli, and N. Engheta, Tunable radiation enhancement and suppression using a pair of photonically doped epsilon-near-zero (ENZ) slabs, *Opt. Lett.* 47(6), 1319 (2022)
36. Y. X. Wang and P. Xu, Spatial heterogeneity of the doping mode: A potential optical reconfiguration freedom of photonic doping epsilon-near-zero media, *Opt. Mater.* 135, 113300 (2023)
37. Y. Li, Z. H. Zhou, Y. J. He, and H. Li, Epsilon-Near-Zero Metamaterials, Cambridge University Press, Cambridge, 2021
38. Z. H. Zhou, and Y. Li, N-port equal/unequal-split power dividers using epsilon-near-zero metamaterials, *IEEE Trans. Microw. Theory Tech.* 69(3), 1529 (2021)
39. H. Li, Z. Zhou, Y. He, W. Sun, Y. Li, I. Liberal, and N. Engheta, Geometry-independent antenna based on epsilon-near-zero medium, *Nat. Commun.* 13(1), 3568 (2022)
40. H. Li, P. Fu, Z. Zhou, W. Sun, Y. Li, J. Wu, and Q. Dai, Performing calculus with epsilon-near zero metamaterials, *Sci. Adv.* 8(30), eabq6198 (2022)
41. M. Coppolaro, M. Moccia, G. Castaldi, N. Engheta, and V. Galdi, Non-Hermitian doping of epsilon-near-zero media, *Proc. Natl. Acad. Sci. USA* 117(25), 13921 (2020)
42. Y. Y. Fu, X. J. Zhang, Y. D. Xu, and H. Y. Chen, Design of zero index metamaterials with *PT* symmetry using epsilon near-zero media with defects, *J. Appl. Phys.* 121(9), 094503 (2017)
43. J. Luo, B. Liu, Z. H. Hang, and Y. Lai, coherent perfect absorption via photonic doping of zero-index media, *Laser Photonics Rev.* 12(8), 1800001 (2018)
44. D. Wang, J. Luo, Z. Sun, and Y. Lai, Transforming zero index media into geometry-invariant coherent perfect absorbers via embedded conductive films, *Opt. Express* 29(4), 5247 (2021)
45. B. Y. Jin and C. Argyropoulos, Nonreciprocal transmission in nonlinear *PT*-symmetric metamaterials using epsilon-near-zero media doped with defects, *Adv. Opt. Mater.* 7(23), 1901083 (2019)
46. P. Bai, K. Ding, G. Wang, J. Luo, Z. Q. Zhang, C. T. Chan, Y. Wu, and Y. Lai, Simultaneous realization of a coherent perfect absorber and laser by zero index media with both gain and loss, *Phys. Rev. A* 94(6), 063841 (2016)
47. Y. Y. Fu, Y. D. Xu, and H. Y. Chen, Zero index metamaterials with *PT* symmetry in a waveguide system, *Opt. Express* 24(2), 1648 (2016)
48. Y. D. Chong, L. Ge, and A. D. Stone, *PT*-symmetry breaking and laser-absorber modes in optical scattering systems, *Phys. Rev. Lett.* 106(9), 093902 (2011)
49. L. S. Li, J. Zhang, C. Wang, N. Zheng, and H. Yin, Optical bound states in the continuum in a single slab with zero refractive index, *Phys. Rev. A* 96(1), 013801 (2017)
50. Y. Y. Fu, Y. D. Xu, and H. Y. Chen, Negative refraction based on purely imaginary metamaterials, *Front. Phys.* 13(4), 134206 (2018)